PCCP

ROYAL SOCIETY OF CHEMISTRY

PAPER

View Article Online
View Journal

Cite this: DOI: 10.1039/d5cp01092f

Influence of hydration, hydroxylation, and doping of TiO_2(110) on the adsorption and decomposition of sarin: a density functional theory investigation†

Yenny Cardona Quintero‡ and Ramanathan Nagarajan *

Received 20th March 2025,
Accepted 22nd July 2025

DOI: 10.1039/d5cp01092f

rsc.li/pccp

Metal oxides are promising candidates for the adsorption and decomposition of chemical warfare agents (CWA) and can be the foundations of novel CWA destruction technologies. In this work, we use density functional theory (DFT) to explore how dry, wet and doped states of the metal oxide TiO_2(110), influence the adsorption and chemical dissociation of the nerve agent, sarin. The DFT calculations show that the dissociative adsorption of sarin is more energetically favored than the molecular adsorption for all dry, wet and doped states of TiO_2(110). The calculated energy barrier for the adsorption of sarin on dry TiO_2(110) showed that sarin is initially adsorbed with a molecular configuration, followed by the dissociative process. For the adsorption of sarin on wet TiO_2, under both hydrated and hydroxylated states, the 0.5 H_2O monolayer (ML) showed the lowest adsorption energy compared to the dry and other wetness levels explored. Finally, the adsorption of sarin on TiO_2(110) doped with Hf exhibited lower adsorption energy and higher charge transfer compared with TiO_2(110) doped with Zr and Ge, as well as the undoped systems. These results demonstrate how hydration, hydroxylation, and doping of TiO_2(110) significantly influence the adsorption and decomposition of sarin on this metal oxide.

1. Introduction

Nerve agents are highly toxic chemicals that continue to pose a threat to military and civilian personnel.[1] The nerve agents are organophosphate (OP) compounds, and their lethality comes from their ability to bind to the acetylcholinesterase (AChE) enzyme, preventing the enzymatic breakdown and regulation of the neurotransmitter acetylcholine (ACh). The resulting accumulation of acetylcholine causes continuous nerve impulses and muscle contractions, and this neurotoxicity can be acute and fatal.[1,2] Sarin (isopropyl methyl phosphono fluoridate, commonly designated as agent GB), is one example of a nerve agent which has been used in terrorist attacks and armed conflicts including the Syrian war, resulting in many fatalities and acute health effects for vast populations. Apart from such weaponization, the residual, undeclared, stockpiles of chemical weapons held by nations, that have not been destroyed despite it being 28 years since the Chemical Weapons Convention,[3] pose an increasing environmental threat to land, water and civilian populations. Therefore, to protect soldier and civilian populations and to decontaminate equipment and infrastructure in the event of a chemical attack and to ensure remediation of environments affected by residual stockpiles of chemical agents, there is an imperative need to develop novel materials that can adsorb and dissociate nerve agents such as sarin into harmless chemicals.

Among the materials considered for the adsorption and dissociation of nerve agents are various metal oxides, which exhibit high stability, large numbers of reactive sites and good selectivity for applications in sensing and decontamination of nerve agents.[4–8] Titanium dioxide has proven to be the leading material for photocatalyst applications.[9–13] Furthermore, metal doping of TiO_2 has been shown to be an effective way to tune electronic and optical properties including decreasing the band gap and extending the absorption into the visible region, which is expected to improve the photocatalytic activity for degradation of chemical warfare agents.[14–17] Cation doping of TiO_2 is also considered a strategy for delaying the deactivation of TiO_2.

Experimental investigations of adsorption and dissociation of nerve agents on metal oxides are necessarily limited due to their high toxicity. To circumvent handling these toxic chemicals, one approach is to conduct experiments using simulants, which are molecules with structures and molecular features similar to the nerve agents but with lower toxicity.[18] Many experimental

US Army Combat Capabilities Development Command Soldier Center, 15 General Greene Avenue, Natick, MA 01760, USA.
E-mail: yenny.p.cardonaquintero.civ@us.navy.mil, Ramanathan.nagarajan.civ@army.mil

† Electronic supplementary information (ESI) available. See DOI: https://doi.org/10.1039/d5cp01092f

‡ Current address: Naval Undersea Warfare Center, Division Newport, Newport, RI 02841, USA.

studies have investigated the adsorption and dissociation of simulants for nerve agents, dimethyl methyl phosphonate (DMMP) being one of the most frequently selected simulants.[19–25] The other approach is to conduct theoretical studies on nerve agents, since this obviously does not involve any toxicity risk and allows one to explore the fundamentals of adsorption and decomposition of nerve agents and other toxic chemicals on different decontaminating material surfaces.

Among theoretical methods, density functional theory (DFT) is probably the most important and widely used tool that allows the exploration of how agent molecules interact with different types of potential decontaminating surfaces. DFT-based first principles methods are essential for exploring novel materials, enabling the theoretical calculation of materials properties and the simulation of interaction mechanisms. DFT computations provide fundamental insights complementing experimental findings by offering physical understanding and guiding experimental design, exploration and screening efforts. Some recent examples of diverse applications for DFT computations include calculations of electronic properties of perylene diimide derivatives to determine the response of electromechanical sensors,[26] the binding energy of amino acids on transition metal dichalcogenides for chemical sensor applications,[27] or the NO adsorption energy on metal chelates for controlling environmental NOx emissions.[28] Using DFT, one can determine the structure, stability and electronic properties of nerve agents[29–38] and simulants[39–51] on metal oxide surfaces, at atomic and molecular scales.

While the experimental and theoretical studies in the literature cited above have provided a wealth of information, there are still important unanswered questions as to how surface impurities such as dopants and factors such as the environmental conditions impact the adsorption and dissociation process of nerve agents on metal oxide surfaces. We address this knowledge gap in this work, selecting the metal oxide TiO_2(110) rutile, which is the most thermodynamically stable phase of TiO_2.[52,53] Using DFT methods, we can provide important insights into the ability of TiO_2 to adsorb and decompose the chemical warfare agent sarin. More importantly we can study the local structure modification through doping titania with different elements and the influence of the environmental conditions including H_2O adsorption on the surface and determine their potential impact on the catalytic activity of TiO_2 for the adsorption and decomposition of sarin.

Dopants can influence the surface properties of TiO_2 because the number of their valency electrons may be different from that of Ti^{4+}, the steric effect related to the different size of the dopant compared to Ti^{4+} or the orbital effect due to the energy levels associated to the dopant not being present on the pristine TiO_2 surface. We selected isovalent dopants (eliminating influence of different numbers of valency electrons) that are of a size similar to Ti, so that the geometry perturbations on titania will be minimal when substitutional doping of a Ti atom with the dopant atom is done. The isovalent dopant elements Hf, Zr and Ge can adopt the same oxidation state to the one of Ti on the TiO_2 structure (4^+) and possess a similar atomic radius[54] (155 pm for Hf and Zr and 125 pm for Ge) compared to Ti (140 pm). They have also been used in experimental studies.[16,17]

We investigated the molecular and dissociative adsorption of sarin on dry, wet and doped TiO_2(110), its stability and structure. The molecular and dissociative adsorption energy of sarin on TiO_2 was calculated using density functional theory, while the nudge elastic band method was used to calculate the energy barrier for the dissociation of sarin on dry TiO_2. The charge transfer was calculated using the Bader charge analysis. We determined the effect of water presence and concentration on the TiO_2 surface for the adsorption and dissociation of sarin. By doping TiO_2 with different elements, we were able to determine the variation in the adsorption energy and charge transfer due to the presence of these dopants on the TiO_2 surface for the adsorption and dissociation of sarin. We found that the hydration, hydroxylation and doping of the TiO_2(110) surface cause significant variations in the adsorption and decomposition behavior of sarin on this metal oxide.

2. Computational methods

Density functional theory calculations were developed using the Perdew–Burke–Ernzerhof generalized gradient approximation (PBE-GGA)[55] and the projected-augmented wave (PAW)[56] approach as implemented in the Quantum Espresso software.[57] van der Waals interactions were also considered through the DFT-D2 method of Grimme.[58] The cutoff kinetic energy for the charge density and wave functions were 350 and 30 Ry, respectively (1 Ry = 1312.75 kJ mol^{-1}), as suggested in the pseudopotentials for the different atom types used in this research.

The charge transfer for the sarin doped TiO_2 system was calculated using the Bader charge analysis.[59] In Bader's approach, space is divided into regions by surfaces that run through minima in the charge density. Specifically, at a point on a dividing surface the gradient of the electron density has no component normal to the surface. The regions bounded by such dividing surfaces are referred to as Bader regions. Each Bader region often contains one nucleus, but this is not necessarily so, sometimes no nucleus is found within a Bader region. By integrating the electronic density within the Bader region where an atom's nucleus is located and possibly adding the electronic charge in nearby regions that do not include a nucleus, the total charge on an atom can be estimated. The computations are carried out using the algorithm developed by Henkelman.[60,61] Using this analysis, the charge for the Sarin molecule, the doped TiO_2 surface, and the doped interface were calculated, with the subsequent charge transfer determined.

2.1. Sarin isolated molecule and TiO_2 slab

To determine the most stable structure of the isolated sarin ($C_4H_{10}FO_2P$) molecule, three initial conformations were selected based on the geometries reported in previous investigations as the most stable structures of the molecule[62–66] and verifying the geometric parameters for the different

conformations. We used a 20 × 20 × 20 Å^3 supercell, relaxing the structures until the parameters reached the convergence criteria to obtain the most stable configuration, while the energy was calculated simultaneously.

The TiO_2 rutile bulk system was modeled as a tetragonal crystal lattice with a mesh of 8 × 8 × 10 *k*-points. The final *a* and *c* lattice parameters for the bulk rutile were obtained as 4.6408 Å and 2.9683 Å, respectively, in agreement with previous theoretical and experimental studies.[39,64] The TiO_2(110) rutile slab structure was built with a surface area of 2 × 4 (13.126 Å × 11.873 Å) with 5 TiO_2 perpendicular layers (corresponding to 80 TiO_2 groups or 240 total atoms) and a 15 Å vacuum region and is hereafter referred to as a 2 × 4 × 5 supercell. The TiO_2(110) rutile structure has been identified as the most thermodynamically stable among the TiO_2 phases with a large number of reactive sites.[67] The dimensions of the 2 × 4 × 5 supercell structure of TiO_2 selected in this study allow us to model the adsorption of the sarin molecule. Such large slab systems prevent modification of the molecular geometry associated with large intermolecular interaction effects and provide better accuracy compared to cluster systems.

2.2. Sarin adsorbed on dry TiO_2(110)

The adsorption of sarin on the TiO_2(110) surface was modeled with a 0.125 monolayer (ML) coverage or 1 molecule of sarin per 8 available Ti atoms. The sarin molecule was placed on top of the TiO_2(110) surface forming an asymmetrical configuration for which a dipole moment correction was required to account for the artificial field in the system. A vacuum region of 15 Å was selected after testing different vacuum lengths and corroborating the stability in the geometry and energy of the sarin–TiO_2 system. The initial adsorption geometries of the sarin molecule on the TiO_2(110) surface were built based on information from previous theoretical and experimental studies that reported the possible structure and geometry of the sarin–TiO_2 system.[13,29,62,64,68] For dissociative adsorption of sarin, molecular groups generated from P–F and P–O bond breakages were considered. In addition, parameters such as bond angles, bond lengths, distance of the molecule to the surface, and the possible formation of monodentate configurations, bidentate configurations or secondary bonds were taken into consideration to model the initial structure (see the ESI† Section A, Fig. S1–S3 for examples of the initial sarin conformations considered).

2.3. Sarin adsorbed on wet TiO_2(110)

The adsorption of sarin on wet TiO_2(110) was explored for hydrated and hydroxylated systems with different water coverages. In the hydrated system, the O of the H_2O molecule bonds with a Ti atom on the surface, while in the hydroxylated system the oxygen atom of an OH^- group bonds with a Ti atom and the remaining H^+ interacts with an O on the TiO_2 surface. The geometries of the TiO_2 hydrated and hydroxylated surfaces were selected to have three different water coverages 0.25, 0.5 and 0.75 H_2O ML, corresponding to 2, 4 and 6 water molecules per 8 available Ti atoms on the top TiO_2 layer. The adsorption of the sarin molecule on the hydrated and hydroxylated surfaces with different water coverage was modeled and then relaxed to obtain the most stable conformation. The initial geometries for the adsorption of sarin on the hydrated and hydroxylated TiO_2 were considered based on the results reported elsewhere[62] for the adsorption of sarin on 0.5 H_2O ML coverage for the hydrated and hydroxylated TiO_2 (see the ESI† Section A, Fig. S4 for examples of the initial sarin conformations considered).

2.4. Sarin adsorbed on doped TiO_2(110)

The adsorption of sarin on TiO_2 doped with Hf, Zr and Ge as a single point dopant was evaluated. One Ti atom from TiO_2 was substituted by a single dopant atom of the elements mentioned. In the atomic position substituted in the first layer, the Ti atom is bonding with the sarin molecule. The single dopant atom was substituted in each one of the five TiO_2 layers at the Ti atom with the same or closer to the *xy* position to the Ti atom of the first layer. This procedure was repeated for each one of the three dopant elements, Hf, Zr and Ge. Additional individual dopant positions in the first TiO_2 layer were also considered with the Hf element substituting the Ti atoms closer to the sarin molecule. The initial conformations for molecular and dissociated sarin were selected as those for the dopant-free system and then subjected to optimization.

3. Results and discussion

3.1. Isolated sarin molecule and TiO_2(110) slab

Three different geometries of the isolated sarin molecule were studied in this work as initial conformations. These geometries were selected based on previous studies which described them as the stable configuration of sarin,[62–66] with some discrepancies about bond angles, bond lengths and in general atomic arrangement of the most stable configuration in the molecule. For the geometries of sarin molecule with conformation 1,[62–64] conformation 2,[65] and conformation 3,[66] the final energies were calculated. The final structures and geometrical parameters for the different conformations of sarin are shown in Fig. 1. The lowest total energy for the sarin molecule was obtained for the conformation 1. Conformation 2 and conformation 3 had a higher total energy with respect to conformation 1, of 0.0709 and 0.0388 eV, respectively. Based on the analysis of the total energy, conformation 1 of the sarin molecule has the highest stability.

In the most preferable conformation of sarin, the P atom is a chiral center, while the F atom and the C_CH_3 group are close to a perpendicular direction with respect to the P–O_C–C_B plane. The F–P–O_C and C_C–C_B–O_C bond angles were obtained as 103° and 109°, respectively, and the P–F, P–O_C and P–O_M bond lengths were 1.59, 1.47 and 1.59 Å, respectively. The final geometric parameters of the most stable conformation 1 of isolated sarin molecules, including some bond lengths and bond angles are reported in Table 1.

For the TiO_2(110) 2 × 4 × 5 supercell, the two bottom layers of the metal oxide supercell were fixed at the TiO_2 bulk position

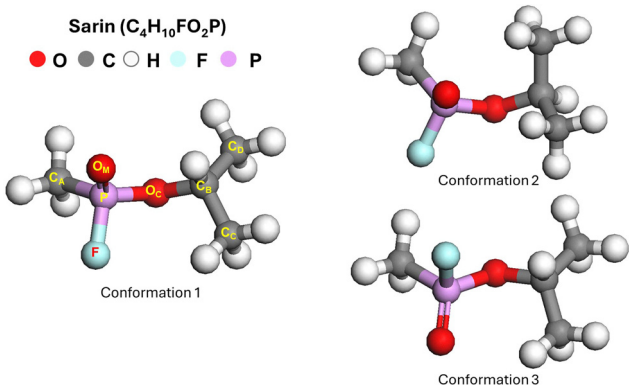

Fig. 1 Final geometry and structures of isolated sarin molecules for three starting conformations. Conformation 1 is determined to be the most stable structure.

Table 1 Geometric parameters for the most stable isolated sarin molecule and the TiO_2(110) 2 × 4 × 5 supercell (labels are depicted in Fig. 1 and Fig. 2, respectively)

Isolated sarin molecule		TiO_2(110) 2 × 4 × 5 supercell	
Bond lengths (Å)		Bond lengths (Å)	
P–F	1.59	Ti_{5fc}–O_{3fc}	1.96
P–O_M	1.47	Ti_{6fc}–O_{2fc}	1.83
P–C_A	1.80	Ti_{6fc}–$O_{3fc\text{-}1}$	2.11
P–O_C	1.59		
O_C–C_B	1.48		
C_B–C_C, C_B–C_D	1.52		
Bond angles (°)		Bond angles (°)	
F–P–O_M	112	Ti_{6fc}–O_{2fc}–Ti_{6fc}	108
F–P–O_C	103	Ti_{6fc}–$O_{3fc\text{-}1}$–Ti_{6fc}	89
O_M–P–C_A	118	Ti_{5fc}–O_{3fc}–Ti_{5fc}	98
C_A–P–O_C	103		
P–O_C–C_B	121		
C_C–C_B–O_C	109		

while the three top layers were allowed to relax. The geometrical parameters of the TiO_2(110) 2 × 4 × 5 supercell are outlined in Table 1 and the corresponding labels are shown in Fig. 2.

In the TiO_2(110) surface, the top and bottom layers have two Ti atom types, the Ti five-fold coordinated (Ti_{5fc}) and the Ti six-fold coordinated (Ti_{6fc}), as well as two O atom types, the O two-fold coordinated (O_{2fc}) and the O three-fold coordinated (O_{3fc}). In Ti_{5fc} and Ti_{6fc} the Ti atom bonds with 5 and 6 O atoms, respectively, while in O_{2fc} and O_{3fc}, the O atom bonds with 2 and 3 Ti atoms, respectively.

3.2. Adsorption and dissociation of sarin on dry TiO_2

The molecular and dissociative adsorption of sarin on the TiO_2(110) 2 × 4 × 5 supercell structure was initially investigated for the clean surface (without impurities or water adsorption). The initial structures were selected based on the information reported in a similar work[62] for the adsorption of sarin on TiO_2. The molecular and dissociative adsorptions of sarin on TiO_2(110) were studied with different initial possible configurations of

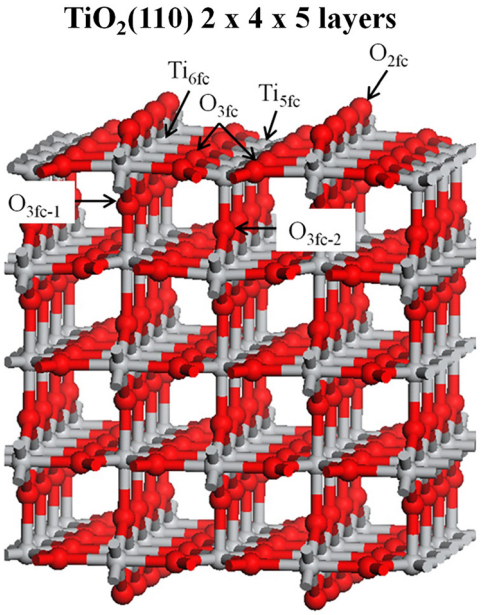

Fig. 2 Final structure of the TiO_2(110) rutile 2 × 4 × 5 supercell. The lattice parameters of the slab are a_{slab} = 6.563 Å and b_{slab} = 2.968 Å. The top and bottom layers have two Ti atom types, five-fold coordinated (Ti_{5fc}) and six-fold coordinated (Ti_{6fc}) and two O atom types, the two-fold coordinated (O_{2fc}) and the three-fold coordinated (O_{3fc}).

sarin on rutile TiO_2(110) in which the sarin molecule interacts with the TiO_2 surface by the formation of a monodentate configuration with Ti–O or F–Ti bonds or a bidentate configuration with the Ti–O and F–Ti bonds. We determined the preferable configuration of the sarin-TiO_2 system through calculation of the adsorption energy for the different conformations explored. The adsorption energy (E_{ads}) for the sarin molecule adsorbed on TiO_2(110) is defined as:

$$E_{ads} = E_{Sarin\text{-}TiO_2(110)} - E_{TiO_2(110)} - E_{Sarin} \quad (1)$$

where $E_{Sarin\text{-}TiO_2(110)}$ is the energy of the sarin–TiO_2(110) system after adsorption, $E_{TiO_2(110)}$ is the energy of the clean TiO_2(110) surface and E_{Sarin} is the energy of the gas phase isolated sarin molecule. The E_{ads} for the most stable adsorbed geometry of sarin on TiO_2(110) was obtained as −1.84 eV and is characterized by the formation of a monodenate covalent bond between the P═O group from sarin and the Ti_{5fc} atom from the TiO_2(110) surface with the formation of several secondary bonds between sarin and the O_{2fc} surface atom of TiO_2(110). The E_{ads} and structure of the most stable configuration for the molecular adsorption of sarin on TiO_2(110) is shown on Fig. 3.

We also considered the dissociative adsorption of sarin on TiO_2(110) with different dissociative products, which was also described in previous reported work.[62] The E_{ads} for the most stable dissociative adsorption of sarin on TiO_2(110) was obtained as −2.70 eV. The final geometry for the dissociative adsorption of the sarin–TiO_2 system was obtained as the dissociation of the F atom from the surface and its adsorption on the TiO_2 surface by the formation of a F–Ti bond. The remaining $C_4H_{10}O_2P^+$ molecule interacts with an O_{2fc} atom on

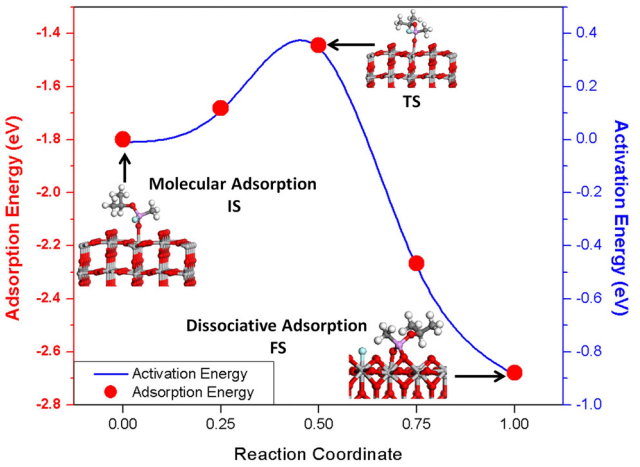

Fig. 3 Calculated adsorption energy and activation energy for the dissociation of sarin on dry TiO_2(110). Inserted in the figure are sarin conformations in the initial state (IS) of molecular adsorption and the final state (FS) of dissociative adsorption. The conformation in the transition state (TS) preceding dissociation is also shown.

the surface forming a bidentate configuration. This final geometry, as well as the E_{ads} for the dissociative adsorption of sarin on TiO_2 are also shown on Fig. 3. The comparison between the E_{ads} values obtained for the most stable configurations of the molecular and dissociative adsorption of sarin on TiO_2 indicates that the dissociative adsorption of sarin is preferred over molecular adsorption. These results, along with the final structures obtained, could indicate the possible mechanism being an initial molecular adsorption of sarin on TiO_2 followed by the dissociation of the molecule, as also suggested by previous experimental studies.[12,13]

To clearly establish the adsorption and dissociative process of sarin on TiO_2(110), the energy barrier between the molecular and dissociative adsorption of the molecule was calculated using the nudge elastic band method. The final geometry for the molecular adsorption of sarin on TiO_2 is considered as the initial state (IS) while the dissociative adsorption configuration of sarin on TiO_2 was identified as the final state (FS). We found that the dissociation of sarin on TiO_2(110) is exothermic with an energy barrier of 0.35 eV at the transition state (TS). The energy barrier and the structure of IS, TS and FS obtained for the adsorption process of sarin on TiO_2 are shown in Fig. 3. The rotation and orientation of the isopropyl group and the F atom in the sarin molecule from the initial state to the transition state, before the dissociation of F, are the main contributions to the energy barrier for sarin dissociation on TiO_2(110). Given the small energy barrier obtained for the dissociation of sarin on TiO_2 and its exothermic nature, we suggest the adsorption mechanism of sarin on TiO_2 as an initial molecular adsorption (observed in IS) with a subsequent dissociation of the F atom and the formation of a bidentate configuration by the remaining molecule as observed in FS in Fig. 3. The adsorption followed by the dissociation of sarin on TiO_2(110) is shown in Fig. 4.

Our computational results agree with previous theoretical and experimental studies on the adsorption of sarin on

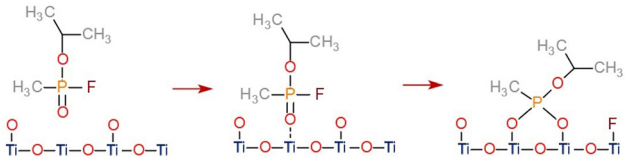

Fig. 4 Molecular adsorption followed by the dissociation of sarin at the P–F bond on dry TiO_2.

different surfaces. The theoretical investigations on the adsorption of sarin on the anatase TiO_2(001) and Al_2O_3 clusters determined the E_{ads} values to be −2.00 eV,[66] and −2.23 eV,[29] respectively. A combined theoretical and experimental work on the adsorption of sarin on SiO_2 also reported values for E_{ads} of −0.82 and −0.95 eV from the experiments and calculations, respectively.[69] A previous experimental work[68] investigating the adsorption of sarin on hydroxylated TiO_2 found that dissociative adsorption of the molecule is preferable with the F atom from sarin interacting with the hydroxyl groups from the surface, facilitating the final dissociation of the fluorine atom and the subsequent formation of a bidentate configuration from the remaining sarin molecule.

3.3. Adsorption and dissociation of sarin on wet TiO_2 with different H_2O ML coverage

The results obtained for the adsorption of sarin on dry TiO_2 indicate that theoretically, the dissociation of the molecule on a dry surface is possible. However, a clean and dry TiO_2 surface is difficult to obtain in practice, under common experimental conditions. Previous experimental study[68] reported the adsorption of sarin on a hydroxylated TiO_2(110) as an initial molecular adsorption process followed by the dissociation of the sarin molecule on the hydroxylated TiO_2(110) surface. Based on a previous investigation[62] on the hydration and hydroxylation of sarin on TiO_2(110) with 0.5 H_2O ML coverage, we selected the most stable molecular and dissociative configurations of sarin on a TiO_2 surface and considered additional levels of H_2O coverage.

To determine the effect of water content on the TiO_2 surface for the adsorption and dissociation of sarin, we compared the E_{ads} for the molecular and dissociative adsorption of sarin on a hydrated and hydroxylated TiO_2(110) surface for three H_2O coverages: 0.25 ML, 0.5ML and 0.75 ML (corresponding to 2, 4 and 6 H_2O molecules of water, respectively, per 8 available Ti_{5fc} atoms on top of the TiO_2 slab). The molecular and dissociative adsorption of sarin on the 0.5 H_2O ML for the hydrated and hydroxylated TiO_2 had the lowest E_{ads} values among the different H_2O coverages, as shown in Fig. 5. In addition, E_{ads} for the dissociative adsorption of sarin on both the hydrated and hydroxylated TiO_2 surfaces were lower compared to E_{ads} for the molecular adsorption, showing a similar tendency to that observed for the adsorption of sarin on dry TiO_2. The comparison of E_{ads} on dry and wet sarin–TiO_2(110) systems showed that the dissociative adsorption of sarin on 0.5 H_2O ML TiO_2, specifically a hydrated surface is the preferable configuration, is in general agreement with the suggestion proposed in a previous experimental study.[68]

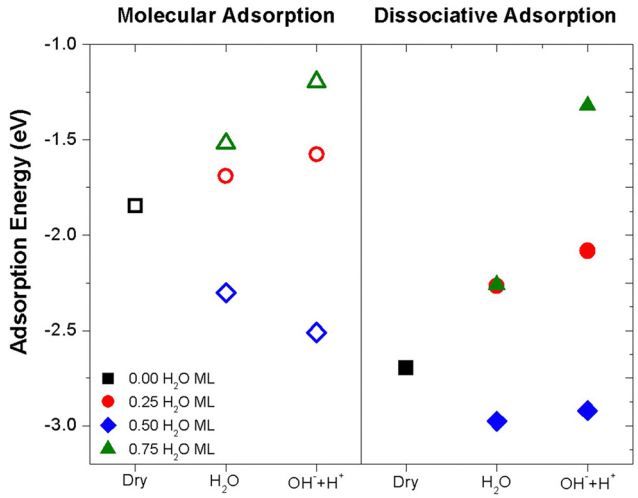

Fig. 5 Calculated adsorption energies for molecular and dissociative adsorption of sarin on dry, hydrated (H_2O) and hydroxylated ($OH^- + H^+$) TiO_2(110). The open symbols correspond to molecular adsorption while the filled symbols correspond to dissociative adsorption.

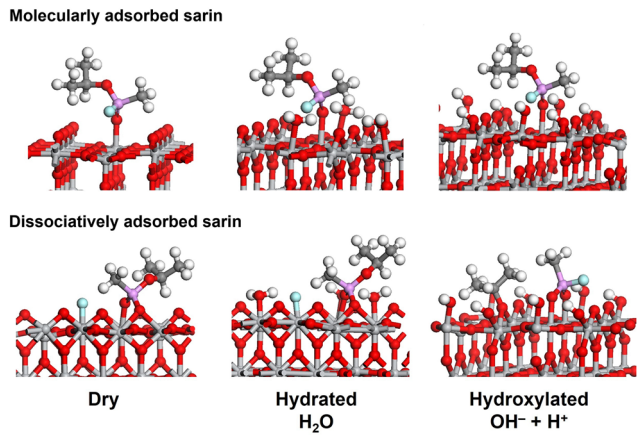

Fig. 6 Structure and geometry of molecularly and dissociatively adsorbed sarin on dry, hydrated (H_2O) and hydroxylated ($OH^- + H^+$) TiO_2(110).

The final geometries for the most stable molecular and dissociative adsorption of sarin on wet (hydrated and hydroxylated) TiO_2 systems are shown on Fig. 6 and these are similar to the ones observed for the dry systems. A schematic of the mechanism of adsorption of sarin on dry and wet TiO_2 for hydrated (H_2O) and hydroxylated ($OH + H^+$) surfaces is provided in the ESI† Section B, Fig. S5.

For the molecular adsorbed structure, the formation of a P═O bond with the TiO_2 surface was more stable, while in the dissociatively adsorbed structure, the F atom dissociates from sarin and is adsorbed on the TiO_2 surface while the remaining molecule forms a bidentate configuration with a O_{2fc} from TiO_2. Additional secondary bonds formed between sarin and the water molecules were observed for the hydrated and hydroxylated systems. The formation of these secondary bonds could have a relevant impact on the stability of the molecular and dissociative adsorption of sarin on wet TiO_2.

A comparison of the number of secondary bonds formed between the different H_2O ML suggests that in the case of the lower H_2O coverage (0.25 ML) the number of secondary bonds between sarin and H_2O or OH groups decreased compared to the 0.5 H_2O ML. In contrast, in the case of higher H_2O coverage (0.75 ML) the presence of additional H_2O or OH groups saturate the Ti_{5fc} available positions preventing the bond formation between Ti and the sarin molecule.

At 0.25 H_2O ML, the chemisorption of sarin on TiO_2 is observed with weak interatomic and intermolecular interactions occurring between sarin and H_2O. At higher degrees of hydration, specifically 0.5 H_2O ML, sarin still exhibits chemisorption on TiO_2 with strong bonds formed between the molecule and the surface. Additionally, there are interatomic interactions occurring between H_2O and the sarin molecules, which could be mostly identified as van der Waals interactions or hydrogen bonding, resulting in lower E_{ads}. As the degree of hydration increases for 0.75 H_2O ML, the H_2O molecules start to compete with sarin for adsorption sites on the titania surface with sarin showing now weaker interaction and mostly physisorption on the TiO_2 surface and consequently higher E_{ads}.

3.4. Adsorption and dissociation of sarin on substitutionally doped TiO_2 with X (X = Hf, Zr or Ge)

Previous experimental studies[4,70–72] have suggested that doping TiO_2 with elements such as Hf, Zr and Ge can increase the degradation rate of chemical warfare agents including soman, VX and sulfur mustard. In the case of sarin, there are no available theoretical or experimental studies, to the best of our knowledge, on the adsorption of sarin on doped TiO_2. To understand the influence of doping TiO_2 on the adsorption and decomposition of sarin, we selected three dopant elements Hf, Zr and Ge to act as substitutional dopants. These elements can adopt the same oxidation state to the one of Ti on the TiO_2 structure (4+) and possess a similar atomic radius[52] (155 pm for Hf and Zr and 125 pm for Ge) compared to Ti (140 pm).

Different orientations of sarin on the TiO_2 surface were considered to account for the possible adsorption configurations of the molecule both in the molecular and dissociative configuration (see the ESI† Section A, Fig. S1–S3 for examples of initial sarin conformations considered, also for the doped TiO_2 system). The specific configurations were selected based on different geometrical parameters for the interface including bond angle, bond length, possible secondary bonds formed, as well as distance and orientation of the molecule respect to the surface.[62] The selection of the most stable adsorption configuration was determined based on the adsorption energy (E_{ads}) values calculated for each system.

3.4.1. Adsorption energy when the dopant atom is in different layers of the supercell. Initially, we doped a single position at a Ti site for each of the five TiO_2 layers when sarin is molecularly and dissociatively adsorbed on the surface. The dopant site at the first layer was selected as the position at which the X dopant (X = Hf, Zr or Ge) is at the Ti_{6fc} site of the TiO_2 surface forming a bond with the sarin molecule. Therefore, the dopant element X is bonding with the O_M atom

(oxygen atom of sarin forming a bond with the surface) of the sarin molecule. The dopant positions for the other layers (between the 2nd and the 5th layer) were selected in the same or closer to the *xy* atomic position chosen for the dopant at the first layer. The configurations obtained as the most stable structures for the molecular and dissociative adsorption of sarin on clean and dry TiO_2, were considered as the initial configurations for sarin on X-doped TiO_2 systems.

The E_{ads} values for the molecular and dissociative adsorption of sarin on doped TiO_2 with the dopants Hf, Zr and Ge were calculated with a similar relationship to eqn (1) and are shown in Fig. 7. The final E_{ads} values are lower when the dopants Hf and Zr are at the first layer of the TiO_2 surface forming a bond with the sarin molecule. The E_{ads} values for the molecular and dissociative adsorption of sarin on Hf-doped TiO_2 were -2.40 and -3.22 eV, respectively. For the case of sarin on Zr-doped TiO_2 the molecular and dissociative adsorption had values of -2.18 and -3.03 eV, respectively, as shown in Fig. 7. When these dopants are positioned at the other TiO_2 layers, the E_{ads} values increase (between 0.3 and 0.5 eV larger) and in some cases are even higher than the undoped systems. In the case of the molecular and dissociative adsorption of sarin on Ge-doped TiO_2, the E_{ads} shows in general a constant tendency with higher values than those of sarin on Hf and Zr-doped TiO_2, as well as the undoped systems.

In terms of the different types of adsorption, the E_{ads} values calculated for the dissociative adsorption of sarin on X-doped TiO_2 are lower than for the molecular adsorption, for all the cases considered. The comparison between the doped and undoped systems showed that the adsorption of sarin on Hf and Zr-doped TiO_2 where the dopant is placed at the first layer is more stable compared with the undoped systems, for the cases of both molecular and dissociative adsorption.

In addition, as the dopant position moves farther away from the surface, and from the sarin molecule, the E_{ads} values are closer to those of the undoped system, indicating that the effect of the dopant becomes more tenuous, as can be expected. For the case of Hf as the dopant, the asymptotic adsorption energy for both molecular and dissociative adsorption, as the layer depth increases is still a little lower than the adsorption energy for the undoped TiO_2. While dopants located deeply within the titania might have a less direct impact compared to surface dopants, they can still influence catalytic activity through electronic and strain effects that extend to the surface. The extent of this influence depends on the material properties, dopant characteristics, and the depth of the dopant within the titania structure. Considering the ionic radius, lattice strain and electronegativity of the different dopant elements Hf, Zr and Ge, compared with Ti in the rutile structure, the combined properties of Hf (small radius and electronegativity) can lead to a more stable structure when doping the rutile TiO_2 material and therefore be a better candidate for the adsorption of sarin compared to the other doped materials. The comparison in the direction of the E_{ads} observed for the three dopant elements indicate that in the case of Hf a surface reconstruction or strain can be present which could lead to variation in the properties compared to the other dopants.

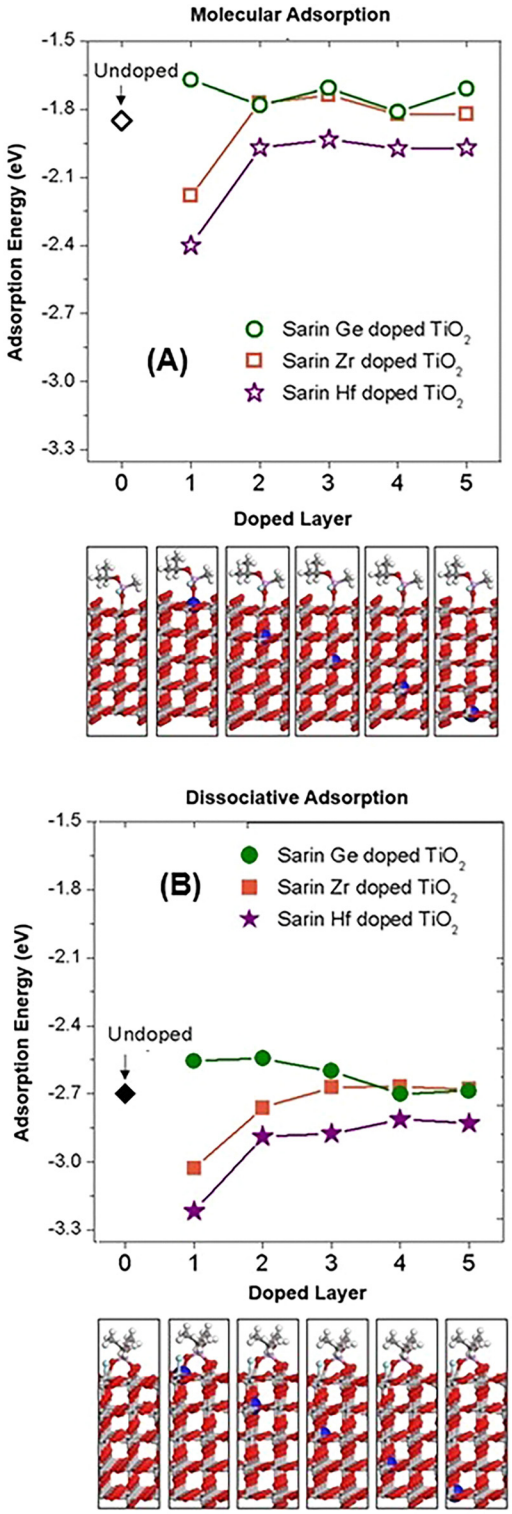

Fig. 7 Molecular (A) and dissociative (B) adsorption energy values for sarin on X-doped TiO_2 systems for X = Hf, Zr or Ge. A single point dopant on each of the five different layers was considered. The dopant position and the corresponding conformation of the adsorbed sarin are also shown.

3.4.2. Charge transfer when the dopant atom is in different layers of the supercell. To determine the relationship between the electronic properties and the stability of the sarin on doped TiO_2 systems, we calculated the charge transfer at the sarin molecule and the dopant atoms when they are at the first layer forming a bond.

The charge transfer (ΔQ) was calculated for each atom of the sarin X-doped TiO_2 systems (X = Hf, Zr or Ge), using the following expression:

$$\Delta Q = Q_{\text{Sarin-X-doped TiO}_2} - Q_{\text{X-doped TiO}_2} - Q_{\text{Sarin}} \qquad (2)$$

where $Q_{\text{Sarin-X-doped TiO}_2}$ is the charge of the sarin X-doped TiO_2 system, $Q_{\text{X-doped TiO}_2}$ is the charge of the X-doped TiO_2 surface with X = Hf, Zr or Ge being at the same position as for the sarin X-doped TiO_2 system and Q_{Sarin} is the charge of the sarin molecule. All these quantities are evaluated at each atom of the specific system. Fig. 8 shows ΔQ at some relevant atoms for the molecularly and dissociatively adsorbed sarin on doped TiO_2 systems for the Hf, Zr and Ge dopants. The atomic positions and labels are depicted at the sarin on the doped TiO_2 structure.

Among the ΔQ values obtained for the different atoms, the results for the dopants (X) and OM draw special attention. The ΔQ values calculated at the dopant atom showed a higher value for sarin on Hf-doped TiO_2 compared with the systems with Zr or Ge. These results apply to both the molecular as well as the dissociative adsorption. In addition, there is a clear difference in the charge transfer direction for the sarin on X-doped TiO_2, when the system is doped with Ge compared to Hf or Zr. In the case of sarin on Hf and Zr-doped TiO_2 the charge transfer is positive, while the same property displays a negative value for sarin on Ge-doped TiO_2.

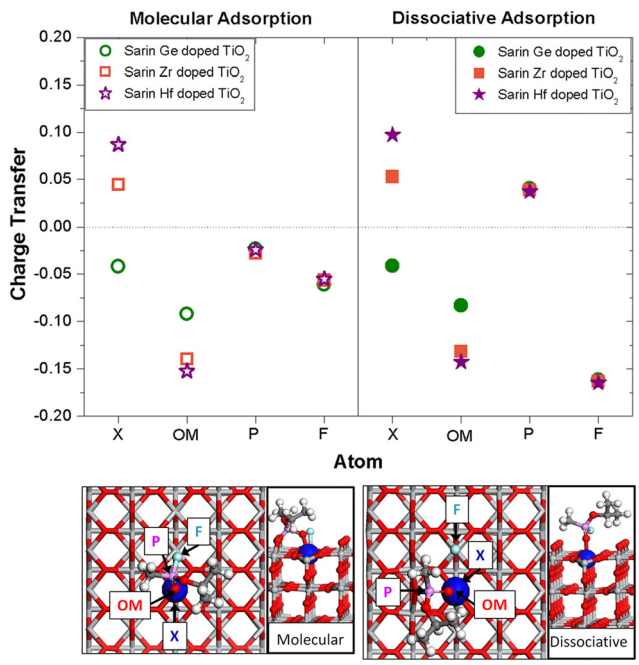

Fig. 8 Charge transfer calculated at different atoms of the molecularly and dissociatively adsorbed sarin on X-doped TiO_2 systems for X = Hf, Zr or Ge. The dopant is on the surface layer.

These results can be interpreted as due to the difference in electronegativities between the different dopants. The electronegativities of Zr and Hf (1.33 and 1.3, respectively) are lower than the electronegativity of Ti (1.54), while the opposite is true for Ge (2.01). The Ge dopant atom has the tendency to attract more electrons when it substitutes the Ti atom of the TiO_2 surface, while Hf and Zr show the opposite effect. A similar comparison for the ΔQ values at the O_M atom of sarin on TiO_2 doped with the different elements show that ΔQ is more negative for the system doped with Hf compared to Zr and Ge. In the X–O_M bond, the charge has a preferred direction toward O due to its higher electronegativity[3,50] and becomes even more negative when the TiO_2 surface is doped with Hf compared to Zr and Ge. Once more, the difference in electronegativity between Ti and the dopant atoms play a role in the charge transfer direction. In addition, the analysis of ΔQ for the P atom shows a different charge transfer direction for the molecular and dissociative configurations with positive and negative values, respectively.

In the molecularly adsorbed configuration, the F atom forms a P–F bond in the sarin molecule, while in the dissociatively adsorbed configuration the F atom dissociates and bonds with a Ti atom at the surface. The breakage of the P–F bond causes a variation not only in the ΔQ value but also in the charge transfer direction at the P atom.

The comparison for sarin on X-doped TiO_2 between the different dopants indicates that the trend observed for the adsorption energy in terms of increasing stability is also observed qualitatively for the charge difference. Sarin on the Hf-doped TiO_2 system with the Hf dopant at the first layer had the lowest E_{ads} (the highest stability) and showed a higher charge transfer, while the E_{ads} had the lowest value for sarin on the Ge-doped TiO_2 system with charge transfer having a lower value and also an opposite direction compared with the Hf-doped system, which suggest that the trend observed for the E_{ads} could have the same origin in the electronic properties of sarin on doped systems.

3.4.3. Adsorption energy and charge transfer when the dopant atom is in different locations on the top layer of the supercell. It was noted earlier in Fig. 7 that the lowest E_{ads} values were obtained for sarin on Hf-doped TiO_2 when the dopant atom is at the first layer, bonding with the adsorbed sarin molecule. Taking this into consideration, we selected the Hf dopant to further explore the adsorption of sarin on Hf-doped TiO_2 with additional dopant positions specifically at the first TiO_2 layer. Fig. 9 shows the additional dopant sites selected at the first layer for the molecular and dissociative adsorption of sarin on Hf-doped TiO_2 and the E_{ads} values for those specific dopant positions.

In the case of the molecular adsorption of sarin on Hf-doped TiO_2, we observe that the E_{ads} values for the additional dopant positions considered (1B, 1C, 1D, 1E, 1F and 1G) are between −1.90 and −2.10 eV which are similar to the E_{ads} of the sarin-TiO_2 undoped system (−1.85 eV) and higher than the value of

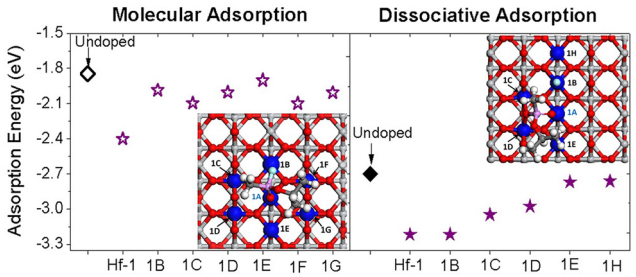

Fig. 9 Calculated adsorption energies for molecular and dissociative adsorption of sarin on Hf-doped TiO_2(110) with Hf at different positions on the first TiO_2 layer (Hf atoms in blue).

−2.4 eV for the dopant position Hf-1 in which case sarin bonds with the dopant Hf. In the case of the dissociative adsorption of sarin on Hf-doped TiO_2, the E_{ads} values range between −3.20 and −2.80 eV with 2 systems being more stable and having the same E_{ads} value (−3.20 eV). These E_{ads} are obtained for sarin on Hf-doped TiO_2 systems when Hf is bonding with the O_M atom (Hf-1, as also described previously) and when Hf is bonding with the F atom dissociated from sarin, corresponding to 1B in Fig. 9.

We calculated the charge transfer at different atomic positions and when the Hf dopant is at the 1B position, we found that ΔQ at Hf is small (0.02 e), while ΔQ at the F atom is negative with a value close to −0.11. In the Hf–F bond, the charge could go in the direction toward the F atom which could be the reason for the small ΔQ value obtained at the Hf atom. The values for ΔQ at O_M and P are around −0.16 and 0.04 eV with the positive charge difference in P due to the dissociation of F from sarin and the charge rearrangement in the remaining molecule. The additional dopant positions also have a lower E_{ads} compared with the undoped system (−2.70 eV), with two positions having values close to −3.0 eV. In these two positions, the O_{2fc} atom bonding with the remaining sarin molecule after dissociation is also forms X–O bonds with the dopant, corresponding to positions 1C and 1D in Fig. 9. The results described here show that not only the dopant element but also the dopant position plays a decisive role in the stability and dissociation of the sarin–TiO_2 system.

4. Conclusions

The molecular and dissociative adsorption of sarin on dry, wet and doped TiO_2(110) surfaces was studied using density functional theory. We found that

(i) For the different cases considered here, the dissociative adsorption of sarin had lower adsorption energy compared against the molecular adsorption, with the F atom dissociating from the sarin molecule and forming a bond with a Ti_{5fc} atom from the surface.

(ii) The energy barrier for the dissociation process of sarin on dry TiO_2 was obtained as 0.35 eV in which an initial molecular adsorption was followed by a dissociative adsorption of sarin on the dry TiO_2 surface.

(iii) The calculation of the adsorption energy for sarin on wet TiO_2 surfaces showed that the dissociative adsorption of sarin on a hydrated TiO_2 with 0.5 H_2O ML coverage was the preferred configuration among the different wet and dry systems considered.

(iv) The adsorption and dissociation of sarin on doped TiO_2 with Hf, Zr and Ge as single point dopants at different layers of the TiO_2 slab was also studied and the calculations showed higher stability for the dissociative adsorption of sarin on Hf-doped TiO_2 compared to Zr and Ge doped systems. The dopant position also had an effect on the stability of sarin on doped TiO_2 systems.

(v) The calculation of the charge transfer at the dopant atom and the sarin molecule for sarin on doped TiO_2 showed the highest value for the system with the highest stability, namely, sarin on Hf-doped TiO_2.

The results obtained in this work suggest that methods such as the hydration, hydroxylation and doping of TiO_2 could represent effective ways to improve the adsorption and dissociation of sarin on this metal oxide and more importantly could facilitate the decontamination process of this highly toxic molecule.

Author contributions

Conceptualization, Y. C. Q., R. N.; methodology and investigation, Y. C. Q.; formal analysis, Y. C. Q., R. N.; writing – original draft preparation, Y. C. Q.; writing – review and editing, Y. C. Q., R. N.; project administration, R. N. All authors have read and agreed to the published version of the manuscript.

Conflicts of interest

The authors declare no conflict of interest.

Abbreviations

Ach	Acetylcholine
AChE	Acetylcholine esterase
CWA	Chemical warfare agent
DFT	Density functional theory
DMMP	Dimethyl methyl phosphonate
GB	Sarin, Isopropyl methyl phosphono fluoridate
ML	Monolayer
OP	Organophosphate
PAW	Projected augmented wave
PBE-GGA	Perdew–Burke–Ernzerhof generalized gradient approximation

Data availability

All original data from this study are included in the article itself and further inquiries can be directed to the corresponding author. Example of an input file for the sarin–TiO_2 system with molecular adsorption is included in the ESI† Section C.

Acknowledgements

This research was conducted as part of the core research at the U.S. Army Combat Capabilities Development Command Soldier Center. The authors acknowledge computational support through the DoD High-Performance Computing Modernization Program. Yenny Cardona Quintero was a National Research Council Postdoctoral Fellow during this project.

References

1 Y. J. Jang, K. Kim, O. G. Tsay, D. A. Atwood and D. G. Churchill, Update 1 of: Destruction and detection of chemical warfare agents, *Chem. Rev.*, 2015, **115**, PR1–PR76.
2 R. Stone, How to defeat a nerve agent, *Science*, 2018, **359**, 23.
3 Chemical Weapons Convention, Organization for the Prohibition of Chemical Weapons, 2025, **https://www.opcw.org/chemical-weapons-convention**.
4 V. Štengl, J. Henych, P. Janoš and M. Skoumal, Nanostructured metal oxides for stoichiometric degradation of chemical warfare agents, *Rev. Environ. Contam. Toxicol.*, 2016, **236**, 239–258.
5 N. Sharma and R. Kakkar, Recent Advancements on warfare agents/metal oxides surface chemistry and their simulation study, *Adv. Mater. Lett.*, 2013, **4**, 508–521.
6 E. D. Davis, W. O. Gordon, A. R. Wilmsmeyer, D. Troya and J. R. Morris, Chemical warfare agent surface adsorption: Hydrogen bonding of sarin and soman to amorphous silica, *J. Phys. Chem. Lett.*, 2014, **5**, 1393–1399.
7 G. W. Wagner, O. B. Koper, E. Lucas, S. Decker and K. J. Klabunde, Reactions of VX, GD, and HD with nanosize CaO: Autocatalytic dehydrohalogenation of HD, *J. Phys. Chem. C*, 2000, **104**, 5118–5123.
8 W. Zhang, A. M. Asiri, D. Liu, D. Du and Y. Lin, Nanomaterial-based biosensors for environmental and biological monitoring of organophosphorus pesticides, *Trends Anal. Chem.*, 2014, **54**, 1–10.
9 T. Li, R. Tsyshevsky, M. McEntee, E. M. Durke, C. Karwacki, E. E. Rodriguez and M. M. Kuklja, Titania nanomaterials for sarin decomposition: Understanding fundamentals, *ACS Appl. Nano Mater.*, 2022, **5**, 6659–6670.
10 C. Tesvara, C. J. Karwacki and P. Sautet, Decomposition of the toxic nerve agent sarin on oxygen vacancy sites of rutile TiO_2(110), *J. Phys. Chem. C*, 2023, **127**, 8006–8015.
11 G. Bazargan, I. V. Schweigert and D. Gunlycke, Adsorption of organophosphate nerve agent VX on the (101) surface of anatase titanium dioxide, *Surf. Sci.*, 2022, **716**, 121957.
12 T. Hirakawa, K. Sato, A. Komano, S. Kishi, C. K. Nishimoto, N. Mera, M. Kugishima, T. Sano, H. Ichinose, N. Negishi, Y. Seto and K. Takeuchi, Experimental study on adsorption and photocatalytic decomposition of isopropyl methylphosphonofluoridate at surface of TiO_2 photocatalyst, *J. Phys. Chem.*, 2010, **114**, 2305–2314.
13 K. Sato, T. Hirakawa, A. Komano, S. Kishi, C. K. Nishimoto, N. Mera, M. Kugishima, T. Sano, H. Ichinose, N. Negishi, Y. Seto and K. Takeuchi, Titanium dioxide photocatalysis to decompose isopropyl methylphosphonofluoridate (GB) in gas phase, *Appl. Catal., B*, 2011, **106**, 316–322.
14 D. R. Sengele, N. Keller, V. Keller, A. Herissan and C. Colbeau-Justin, Ta-doped TiO_2 as photocatalyst for UV-A activated elimination of chemical warfare agent simulant, *J. Catal.*, 2016, **334**, 129–141.
15 C. S. Cao, W. Liu, A. Ma, X. Jiao, Y. Yang, J. Li and F. Fu, Single-atom Pt-decorated TiO_2 nanotubes for boosted photocatalytic degradation of chemical warfare agents, *ACS Sustainable Chem. Eng.*, 2025, **13**, 6379–6387.
16 V. Štengl, T. M. Grygar, F. Opluštil and T. Němec, Ge^{4+} doped TiO_2 for stoichiometric degradation of warfare agents, *J. Hazard. Mater.*, 2012, **227**, 62–67.
17 Z. Shen, J. Y. Zhong, N. N. Chai, X. He, J. Z. Zang, H. Xu, X. Y. Han and P. Zhang, Evolution of microstructural defects of TiO2 nanocrystals by Zr^{4+} or/and Ge^{4+} doping lead to high disinfection efficiency for CWAs, *Chem. Phys. Lett.*, 2017, **678**, 146–152.
18 J. Lavoie, R. Srinivasan and R. Nagarajan, Using cheminformatics to find simulants for chemical warfare agents, *J. Hazard. Mater.*, 2011, **194**, 85–91.
19 C. N. Rusu and J. T. Yates, Adsorption and decomposition of dimethyl methylphosphonate on TiO_2, *J. Phys. Chem. B*, 2000, **104**, 12292–12298.
20 D. A. Panayotov and J. R. Morris, Uptake of a chemical warfare agent simulant (DMMP) on TiO_2: Reactive adsorption and active site poisoning, *Langmuir*, 2009, **25**, 3652–3658.
21 D. A. Panayotov and J. R. Morris, Thermal decomposition of a chemical warfare agent simulant (DMMP) on TiO_2: Adsorbate reactions with lattice oxygen as studied by infrared spectroscopy, *J. Phys. Chem. C*, 2009, **113**, 15684–15691.
22 J. Zhou, S. Ma, Y. C. Kang and D. A. Chen, Dimethyl methylphosphonate decomposition on titania-supported Ni clusters and films: A comparison of chemical activity on different Ni surfaces, *J. Phys. Chem. B*, 2004, **108**, 11633–11644.
23 J. Zhou, K. Varazo, J. E. Reddic, M. L. Myrick and D. A. Chen, Decomposition of dimethyl methylphosphonate on TiO_2 (110): Principal component analysis applied to X-ray photoelectron spectroscopy, *Anal. Chim. Acta*, 2003, **496**, 289–300.
24 A. R. Wilmsmeyer, W. O. Gordon, E. D. Davis, D. Troya, B. A. Mantooth, T. A. Lalain and J. R. Morris, Infrared spectra and binding energies of chemical warfare nerve agent simulants on the surface of amorphous silica, *J. Phys. Chem. C*, 2013, **117**, 15685–15697.
25 P. Janos, P. Kuran, M. Kormunda, V. Stengl, T. M. Grygar, M. Dosek, M. Stastny, J. Ederer, V. Pilarova and L. Vrtoch, Cerium dioxide as a new reactive sorbent for fast degradation of parathion methyl and some other organophosphates, *J. Rare Earths*, 2014, **32**, 360–370.
26 A. Tiwari, V. Adepu, R. S. Fernandes, N. Dey, P. Sahatiya and S. Kanungo, Perylene diimide architecture-based electromechanical sensors: a systematic experimental and theoretical framework for the comparative analysis and study of the transduction mechanism, *Mater. Adv.*, 2024, **5**, 9243–9258.
27 A. Tiwari, H. V. Barkale, N. Harshini, S. Chennareddy, N. Dey and S. Kanungo, Phenylalanine and tyrosine

interactions with the WSe2 nanosheet: A comparative analysis based on DFT calculation and experimental confirmation, *J. Phys. Chem. C*, 2025, **129**, 1769–1778.
28 H. J. Cho, S. H. Kim, J. Kang, K. Cho, H. Y. Lee, H. Kim, H. K. Ju, J. W. Choi, S. G. Kim, S. G. Oh, C. W. Lee and H. C. Yoon, Experimental and DFT studies on the equilibrium properties, kinetics, and mechanism of nitric oxide removal using metal-EDTA and ferrous thiochelates, *Chem. Eng. J.*, 2022, **431**, 134010.
29 V. M. Bermudez, Computational study of environmental effects in the adsorption of DMMP, Sarin, and VX on γ-Al_2O_3: Photolysis and surface hydroxylation, *J. Phys. Chem. C*, 2009, **113**, 1917–1930.
30 A. Michalkova, M. Ilchenko, L. Gorb and J. Leszczynski, Theoretical study of the adsorption and decomposition of sarin on magnesium oxide, *J. Phys. Chem. B*, 2004, **108**, 5294–5303.
31 A. Michalkova and J. Leszczynski, Interactions of nerve agents with model surfaces: Computational approach, *J. Vac. Sci. Technol., A*, 2010, **28**, 1010–1017.
32 B. N. Papas, I. D. Petsalakis, G. Theodorakopoulos and J. L. Whitten, CI and DFT studies of the adsorption of the nerve agent sarin on surfaces, *J. Phys. Chem. C*, 2014, **118**, 23042–23048.
33 R. Wang, B. Wang, A. S. Abdullahi and H. Fan, Understanding the prototype catalyst TiO_2 surface with the help of density functional theory calculation, *Comput. Mol. Sci.*, 2024, **14**, e1686.
34 P. Janos, J. Henych, O. Pelant, V. Pilarova, L. Vrtoch, M. Kormunda, K. Mazanec and V. Stengl, Cerium oxide for the destruction of chemical warfare agents: A comparison of synthetic routes, *J. Hazard. Mater.*, 2016, **304**, 259–268.
35 V. S. Vaiss, I. Borges and A. A. Leit, Sarin degradation using brucite, *J. Phys. Chem. C*, 2011, **115**, 24937–24944.
36 A. Michalkova, J. Martinez, O. A. Zhikol, L. Gorb, O. V. Shishkin, D. Leszczynska and J. Leszczynski, Theoretical study of adsorption of sarin and soman on tetrahedral edge clay mineral fragments, *J. Phys. Chem. B*, 2006, **110**, 21175–21183.
37 A. Michalkova, Y. Paukku, D. Majumdar and J. Leszczynski, Theoretical study of adsorption of tabun on calcium oxide clusters, *Chem. Phys. Lett.*, 2007, **438**, 72–77.
38 L. Yang, D. Tunega, L. Xu, N. Govind, R. Sun, R. Taylor, H. Lischka, W. A. Dejong and W. L. Hase, Comparison of cluster, slab, and analytic potential models for the dimethyl methylphosphonate (DMMP)/TiO_2(110) intermolecular interaction, *J. Phys. Chem. C*, 2013, **117**, 17613–17622.
39 V. M. Bermudez, Ab initio study of the interaction of dimethyl methylphosphonate with rutile (110) and anatase (101) TiO_2 surfaces, *J. Phys. Chem. C*, 2010, **114**, 3063–3074.
40 V. M. Bermudez, First-principles study of adsorption of dimethyl methylphosphonate on the TiO_2 anatase (001) surface: Formation of a stable titanyl (Ti = O) site, *J. Phys. Chem. C*, 2011, **115**, 6741–6747.
41 V. M. Bermudez, Computational study of the adsorption of dimethyl methylphosphonate (DMMP) on the (010) surface of anatase TiO_2 with and without faceting, *Surf. Sci.*, 2010, **604**, 706–712.
42 Y. Paukku, A. Michalkova and J. Leszczynski, Adsorption of dimethyl methylphosphonate and trimethyl phosphate on calcium oxide: An ab initio study, *Struct. Chem.*, 2008, **19**, 307–320.
43 J. Quenneville, R. S. Taylor and A. C. T. van Duin, Reactive molecular dynamics studies of DMMP adsorption and reactivity on amorphous silica surfaces, *J. Phys. Chem. C*, 2010, **114**, 18894–18902.
44 M. R. Housaindokht and N. Zamand, A DFT study of associative and dissociative chemical adsorption of DMMP onto SnO_2(110) surface nanocluster, *Struct. Chem.*, 2015, **26**, 87–96.
45 D. A. Trubitsyn and A. V. Vorontsov, Molecular and reactive adsorption of dimethyl methylphosphonate over (001) and (100) anatase clusters, *Comput. Theor. Chem.*, 2013, **1020**, 63–71.
46 A. Kiselev, A. Mattson, M. Andersson, A. E. C. Palmqvist and L. Osterlund, Adsorption and photocatalytic degradation of diisopropyl fluorophosphate and dimethyl methylphosphonate over dry and wet rutile TiO_2, *J. Photochem. Photobiol., A*, 2006, **184**, 125–134.
47 M. B. Mitchell, V. N. Sheinker and E. A. Mintz, Adsorption and decomposition of dimethyl methylphosphonate on metal oxides, *J. Phys. Chem. B*, 1997, **101**, 11192–11203.
48 A. R. Head, R. Tsyshevsky, L. Trotochaud, Y. Yu, L. Kyhl, O. Karslıoğlu, M. M. Kuklja and H. Bluhm, Adsorption of dimethyl methylphosphonate on MoO_3: The role of oxygen vacancies, *J. Phys. Chem. C*, 2016, **120**, 29077–29088.
49 L. Trotochaud, R. Tsyshevsky, S. Holdren, K. Fears, A. R. Head, Y. Yu, S. Pletincx, B. Eichhorn, M. Zachariah and M. M. Kuklja, *et al.*, Spectroscopic and computational investigation of room-temperature decomposition of a chemical warfare agent simulant on polycrystalline cupric oxide, *Chem. Mater.*, 2017, **29**, 7483–7496.
50 I. V. Schweigert and D. Gunlycke, Hydrolysis of dimethyl methylphosphonate by the cyclic tetramer of zirconium hydroxide, *J. Phys. Chem. A*, 2017, **121**, 7690–7696.
51 G. Wang, C. Sharp, A. M. Plonka, Q. Wang, A. I. Frenkel, W. Guo, C. Hill, C. Smith, J. Kollar, D. Troya and J. R. Morris, Mechanism and kinetics for reaction of the chemical warfare agent simulant, DMMP(g), with Zirconium (IV) MOFs: An ultrahigh-vacuum and DFT study, *J. Phys. Chem. C*, 2017, **121**, 11261–11272.
52 S. J. Smith, R. Stevens, S. Liu, G. Li, A. Navrotsky, J. Boerio-Goates and B. F. Woodfield, Heat capacities and thermodynamic functions of TiO_2 anatase and rutile: Analysis of phase stability, *Am. Mineral.*, 2009, **94**, 236–243.
53 Z. H. Cui, F. Wu and H. Jiang, First-principles study of relative stability of rutile and anatase TiO_2 using the random phase approximation, *Phys. Chem. Chem. Phys.*, 2016, **18**, 29914–29922.
54 J. C. Slater, Atomic radii in crystals, *J. Chem. Phys.*, 1964, **41**, 3199–3205.
55 J. Perdew, J. Chevary, S. Vosko, K. Jackson, M. Pederson, D. Singh and C. Fiolhais, Atoms, molecules, solids, and surfaces: Applications of the generalized gradient approximation for

exchange and correlation, *Phys. Rev. B: Condens. Matter Mater. Phys.*, 1992, **46**, 6671–6687.
56 P. E. Blöchl, Projector augmented-wave method, *Phys. Rev. B: Condens. Matter Mater. Phys.*, 1994, **50**, 17953–17979.
57 P. Giannozzi, S. Baroni, N. Bonini, M. Calandra, R. Car, C. Cavazzoni, D. Ceresoli, G. L. Chiarotti, M. Cococcioni and I. Dabo, *et al.*, QUANTUM ESPRESSO: A modular and open-source software project for quantum simulations of materials, *J. Phys.: Condens. Matter*, 2009, **21**, 395502.
58 S. Grimme, Semiempirical GGA-type density functional constructed with a long-range dispersion correction, *J. Comput. Chem.*, 2006, **27**, 1787–1799.
59 R. F. W. Bader, *Atoms in Molecules: A Quantum Theory*, Clarendon Press, Oxford, 1994.
60 G. Henkelman, A. Arnaldsson and H. Jónsson, A fast and robust algorithm for Bader decomposition of charge density, *Comput. Mater. Sci.*, 2006, **36**, 354–360.
61 Henkelman Group Code for Bader Charge Analysis, 2023. **https://theory.cm.utexas.edu/henkelman/code/bader/**.
62 Y. Cardona Quintero and R. Nagarajan, Molecular and dissociative adsorption of DMMP, sarin and soman on dry and wet TiO_2(110) using density functional theory, *Surf. Sci.*, 2018, **675**, 26–35.
63 A. Kaczmarek, L. Gorb, A. J. Sadlej and J. Leszczynski, Sarin and soman: Structure and properties, *Struct. Chem.*, 2004, **15**, 517–525.
64 X. Shan, J. C. Vincent, S. Kirkpatrick, M. D. Walker, M. R. Sambrook and D. C. Clary, A combined theoretical and experimental study of sarin (GB), *J. Phys. Chem. A*, 2017, **121**, 6200–6210.
65 T. Ash, T. Debnath, T. Banu and A. K. Das, Exploration of unimolecular gas-phase detoxication pathways of sarin and soman: A computational study from the perspective of reaction energetics and kinetics, *Chem. Res. Toxicol.*, 2016, **29**, 1439–1457.
66 N. Q. Le, C. E. Ekuma, B. I. Dunlap and D. Gunlycke, First-principles calculations of sarin adsorption on anatase surfaces, *J. Phys. Chem. C*, 2018, **122**, 2832–2839.
67 S. Tan and B. Wang, Active Sites for Adsorption and reaction of molecules on rutile TiO_2(110) and anatase TiO_2(001) surfaces, *Chin. J. Chem. Phys.*, 2015, **28**, 383–395.
68 C. J. Howard, T. M. Sabine and F. Dickson, Structural and thermal parameters for rutile and anatase, *Acta Crystallogr., Sect. B*, 1991, **47**, 462–468.
69 D. C. Taylor, K. Runge, M. G. Cory, D. S. Burns, J. L. Vasey, J. D. Hearn, K. Griffith and M. V. Henley, Surface binding of organophosphates on silica: Comparing experiment and theory, *J. Phys. Chem. C*, 2013, **117**, 2699–2708.
70 V. Štengl, S. Bakardjieva, N. Murafa and F. Opluštil, Zirconium doped titania: Destruction of warfare agents and photocatalytic degradation of orange 2 dye, *Open Process Chem. J.*, 2008, **1**, 1–7.
71 V. Štengl, S. Bakardjieva, N. Murafa, F. Opluštil, L. Österlund, A. Mattsson and P. O. Andersson, Warfare agents degradation on zirconium doped titania, *Microsc. Microanal.*, 2009, **15**, 1038–1039.
72 V. Štengl, T. M. Grygar, F. Opluštil and T. Nemec, Ge^{4+} doped TiO_2 for stoichiometric degradation of warfare agents, *J. Hazard. Mater.*, 2012, **227–228**, 62–67.

